

## Dynamic behavior overview of three conventional dc/dc converters used in PV MPPT system

Hamza Snani <sup>\*</sup>, Mohamed Amarouayache <sup>†</sup> and Aissa Bouzid <sup>‡</sup>

Laboratoire d'Electrotechnique de Constantine, Département d'Electrotechnique  
Université Constantine 1, 25000 Constantine, Algeria

(reçu le 20 Mai 2017 - accepté le 30 Juin 2017)

**Abstract** - *To improve the performances of such perturbative maximum power point tracking (MPPT) algorithm, the real-time optimization of the algorithm designed parameters is used. Such optimization depends on the dynamic behavior of the whole photovoltaic (PV) MPPT system, and more especially, on that of the adopted dc/dc converter topology, which is used to realize the MPPT function. Therefore, the present paper shows an analytical study about the dynamic behavior of three conventional dc/dc converter topologies: boost, buck and buck-boost. For that, we establish the small-signal model for three cases of PV MPPT system that are composed each one with each of the above topologies, and then the transfer functions in the Laplace domain are drawn. In this approach, the dynamic behavior is defined by the natural frequency and damping factor parameters of the above systems. The comparison based on the variation of these two parameters, allows us having an overview about the dynamic behavior of the under study systems for the aim to implement a more efficient real-time MPPT algorithm.*

**Résumé** - *Pour améliorer les performances d'un tel algorithme perturbative suivi du point de puissance maximale (SPPM), l'optimisation en temps réel des paramètres d'algorithme conçus est utilisée. Une telle optimisation dépend du comportement dynamique de tout le système photovoltaïque (PV) du SPPM et plus particulièrement, sur celui de la topologie de convertisseur dc/dc adoptée, qui est utilisée pour réaliser la fonction de SPPM. Donc, le papier présent montre une étude analytique du comportement dynamique de trois topologies conventionnelles des convertisseurs dc/dc: boost, buck et buck-boost. Pour cela, nous établissons le modèle des petit signaux pour trois cas du système de PV SPPM qui sont composés chacun avec chacune de la topologie ci-dessus et ensuite les fonctions de transfert dans le domaine de Laplace sont développées. Dans cette approche, le comportement dynamique est défini par la fréquence naturelle et le facteur d'amortissement. La comparaison basée sur la variation de ces deux derniers paramètres, nous permet ayant une vue d'ensemble du comportement dynamique des systèmes en train d'étudier.*

**Keywords:** Photovoltaic MPPT system - Modeling - dc/dc converter topologies - Maximum power point (MPP) - Damping factor - Natural frequency.

### 1. INTRODUCTION

Maximum power point tracking (MPPT) techniques are used to harvest the maximum amount of power which the photovoltaic (PV) source can product, since this nonlinear electrical source exhibits under a given solar irradiation and ambient temperature levels, a voltage-current ( $V-I$ ) characteristic with a unique point called maximum power point (MPP).

Due principally to the variation of the solar irradiation level, which can have a rate of  $100 \text{ W/m}^2/\text{s}$  [1], the MPP is subjected to move rapidly and randomly in the  $V-I$  plane, and hence the efficiency of the used MPPT algorithm can be examined.

---

\* h mz\_s nani@yahoo.fr

† amarouayachemohamed@yahoo.fr

‡ you.bouzid@yahoo.fr

The perturbative MPPT algorithms are widely used for that purpose of tracking, among them the popular ones such as the Perturb and Observe (P&O) and Incremental Conductance (INC) techniques [2]. The efficiency of such technique is translated with its performances under both of transient and steady state responses of the PV system operating point.

Although the use of a fixed algorithm designed parameters (i.e. fixed perturbation amplitude  $\Delta d$  of the duty cycle  $d$  and regularly sampling frequency  $T_s$ ) is simple method to track the MPP, the algorithm performances will not be optimized as the continuously moving of the PV system operating point, and in the critical case (i.e. rapidly variation of the irradiation), the algorithm can be confused. Therefore, and for more harvesting of the instantaneous maximum power, which the PV source can product under a given operating conditions, the real-time optimization of the algorithm parameters is implemented [3].

In [2], an in-depth theoretical analysis is proposed which aims to optimize the performances of P&O algorithm; it consisted of tuning the algorithm parameters to the dynamic behavior of the system (PV array + converter) using a developed formulas. From another hand, the authors in [3] used the latter formulas for the real-time optimization of the formulas for the real-time optimization of the algorithm sampling frequency ( $T_s$ ) according to the transient response of the controlled PV MPPT parameter.

As in general, the controlled parameter in PV MPPT system is the output PV voltage ( $v_{pv}$ ) due to its advantageous which are clearly described in [4], it is desired that ( $v_{pv}$ ) be characterized with a fast transient response when the MPPT action (i.e. when the change in  $d$  happen with a step  $\Delta d$ ), and that for the aim to construct a more optimized real-time algorithm either in the transient or steady state responses. In fact, the transient response behavior of  $v_{pv}$  depends on the whole PV MPPT system dynamic, and more especially, on that of the used dc/dc converter [2, 3].

Therefore, the present paper shows an analytical study about the dynamic behavior of three conventional dc/dc converter topologies: boost, buck and buck-boost. For that, we establish the small-signal model for three cases of PV MPPT system that are composed each one with each of the above topologies (**Table 1**), then the transfer functions ( $F_{v_{pv},d}$ ), which relate the MPPT control parameter ( $d$ ) to the output PV voltage ( $v_{pv}$ ), in the Laplace domain, are set with an approximation of a second order system from a third order one, on the contrary of what is usually done, where the second order system is assumed since the usually connected load type to the output of the used dc/dc converter is a battery, as in [2, 5].

In this approach, the dynamic behavior is defined by the natural frequency ( $\omega_0$ ) and damping factor ( $\xi$ ) parameters which characterize the different systems. The comparison based on the variation of these two parameters, allows us having an overview about the dynamic behavior of the considered PV MPPT systems, and more exactly, the transient response of the controlled MPPT parameter ( $v_{pv}$ ), for the aim to choice the more adequate dc/dc topology to use for real-time perturbative MPPT algorithms.

The paper is organized as follows: In section 2, the modelling of the considered systems is given based on the small signal model and the transfer function concept.

Criteria of the transient response are given in section 3. The results of analytical studies and discussions are shown in section 4. Finally section 5 is devoted to conclusion.

## 2. MODELING OF THE DIFFERENT SYSTEMS

Beginning with the differential equations which governing the dynamics of the state vector of each of the above PV MPPT systems, the small-signal averaged models are obtained as in the subsection A, then in B, the transfer functions ( $F_{V_{pv,d}}$ ) are developed, and there mathematical simplification idea to the second order from a third order one is used now with the PV MPPT system when using the buck and buck-boost converter topologies, and that, after used it with the boost converter [6].

**Table 1:** Considered PV MPPT systems using three conventional dc/dc converter topologies

Type of converter	Scheme of PV MPPT system
Boost	
Buck	
Buck-Boost	

### 2.1 Small-signal model

The equivalent circuit of each of the used dc/dc converter topologies (figure 1 as an example) is constituted with the passive components ( $L$ ,  $C_{pv}$  and  $C_0$ ), which are assumed as ideal and sized away to have a continuous conduction mode (CCM) [5], and the switching cell ( $S$  and  $D$ ), which is supposed without losses (zero on-state voltage drops, zero off-state currents, and instantaneous commutation between the on and off states) [7].

For these considerations, and for the pulse width modulation (PWM) control, there are two stable configurations which appear every switching period ( $T_{sw}$ ; 1) when S is switched-on and D is switched-off in the interval time  $0 \leq t_{on} \leq dT_{sw}$ ; 2) when S is switched-off and D is switched-on in the interval time  $dT_{sw} \leq t_{off} \leq T_{sw}$  where d is the duty cycle ( $d = t_{on} / T_{sw}$ ).

The state variables according to these configurations are:

•Using the **boost** topology

$$\begin{cases} \frac{dv_{pv}}{dt} = -\frac{1}{C_p v_{rpv}} v_{pv} - \frac{1}{C_p v} iL \\ \frac{diL}{dt} = \frac{1}{L} v_{pv} - \frac{1-s}{L} v_0 \\ \frac{dv_0}{dt} = \frac{1-s}{C_0} iL - \frac{1}{C_0 R_0} v_0 \end{cases} \tag{1}$$

•Using the **buck** topology

$$\begin{cases} \frac{dv_{pv}}{dt} = -\frac{1}{C_p v_{rpv}} v_{pv} - \frac{1}{C_p v} iL \\ \frac{diL}{dt} = \frac{s}{L} v_{pv} - \frac{1}{L} v_0 \\ \frac{dv_0}{dt} = \frac{1}{C_0} iL - \frac{1}{C_0 R_0} v_0 \end{cases} \tag{2}$$

•Using the **buck-boost** topology

$$\begin{cases} \frac{dv_{pv}}{dt} = -\frac{1}{C_p v_{rpv}} v_{pv} - \frac{1}{C_p v} iL \\ \frac{diL}{dt} = \frac{s}{L} v_{pv} - \frac{1-s}{L} v_0 \\ \frac{dv_0}{dt} = \frac{1-s}{C_0} iL - \frac{1}{C_0 R_0} v_0 \end{cases} \tag{3}$$

The sets of equations (1), (2) and (3) are the state variables of the under study three systems when using the boost, buck and buck-boost topologies, respectively. The parameter  $r_{pv}$  is the dynamic resistance, which is defined as the ratio of the small change in voltage to that in current of the PV module ( $r_{pv} = \hat{v}_{pv} / \hat{i}_{pv}$ ) [2, 5]. The s symbol is the time-dependent switching variable, which is defined as in (4). Other symbols refer to figure 1.

$$s(t) = \begin{cases} 1 & \text{For S is switched - on} \\ 0 & \text{For S is switched - off} \end{cases} \tag{4}$$

Equations (1), (2) and (3) can be represented with the small-signal averaged state-space model [7], [9] as in the following:

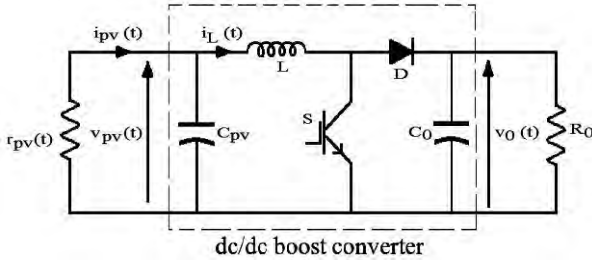


Fig. 1: Example of the equivalent circuit of PV MPPT system using the boost converter

•Using the **boost** topology

$$\frac{d}{dt} \begin{pmatrix} \hat{v}_{PV} \\ i_L \\ v_0 \end{pmatrix} = \begin{bmatrix} \frac{-1}{(C_{pv}r_{pv})} & -\frac{1}{C_{pv}} & 0 \\ \frac{1}{L} & 0 & -\frac{(1-d)}{L} \\ 0 & \frac{(1-d)}{C_0} & -\frac{1}{(C_0R_0)} \end{bmatrix} \begin{pmatrix} \hat{v}_{PV} \\ i_L \\ v_0 \end{pmatrix} + \begin{pmatrix} 0 \\ \frac{V_{pvE}}{L(1-d)} \\ -\frac{V_{pvE}}{C_0r_{pv}} \end{pmatrix} (\hat{d}) \quad (5)$$

•Using the **buck** topology

$$\frac{d}{dt} \begin{pmatrix} \hat{v}_{PV} \\ i_L \\ v_0 \end{pmatrix} = \begin{bmatrix} \frac{-1}{(C_{pv}r_{pv})} & -\frac{d}{C_{pv}} & 0 \\ \frac{d}{L} & 0 & -\frac{1}{L} \\ 0 & \frac{1}{C_0} & -\frac{1}{(C_0R_0)} \end{bmatrix} \begin{pmatrix} \hat{v}_{PV} \\ i_L \\ v_0 \end{pmatrix} + \begin{pmatrix} -\frac{V_{pvE}}{dC_{pv}r_{pv}} \\ \frac{V_{pvE}}{L} \\ 0 \end{pmatrix} (\hat{d}) \quad (6)$$

•Using the **buck-boost** topology

$$\frac{d}{dt} \begin{pmatrix} \hat{v}_{PV} \\ i_L \\ v_0 \end{pmatrix} = \begin{bmatrix} \frac{-1}{(C_{pv}r_{pv})} & -\frac{d}{C_{pv}} & 0 \\ \frac{d}{L} & 0 & -\frac{(1-d)}{L} \\ 0 & \frac{(1-d)}{C_0} & -\frac{1}{(C_0R_0)} \end{bmatrix} \begin{pmatrix} \hat{v}_{PV} \\ i_L \\ v_0 \end{pmatrix} + \begin{pmatrix} -\frac{V_{pvE}}{dC_{pv}r_{pv}} \\ \frac{V_{pvE}(1-2d)}{(1-d)L} \\ -\frac{V_{pvE}}{dC_0r_{pv}} \end{pmatrix} (\hat{d}) \quad (7)$$

In (5), (6) and (7), the variables with a hat are small ac variations about the equilibrium operating point,  $V_{pvE}$  is the equilibrium value of the output PV voltage.

## 2.2 Transfer function and the obtained second order system

By applying the Laplace transform to (5), (6) and (7), the small-signal control to the PV module voltage transfer function ( $F_{v_{pv},d}$ ) is obtained for the three cases of **Table 1** as shown in (8), (9) and (10) at the top of the next page.

According to control theory of linear systems, the dynamic behavior of the obtained transfer functions strongly depends on the nature of the poles of the denominator  $D(s)$ . We note that this last one is a third order polynomial for each of the three systems.

To facilitate the study of the dynamic behavior, the idea was to get a comparable system to a second order in the general form [6]:

$$D(s) = s^2 + 2\omega_0\xi s + \omega_0^2 \tag{8}$$

Where the natural frequency  $\omega_0$  characterizes the time response (i.e. the good variations of  $\omega_0$  provide a fast transient response) since the damping factor  $\xi$  characterizes the oscillation during the transient response (i.e. the good variations of  $\xi$  provide a well damped system).

The pair of complex conjugate poles then  $\Delta D(s) > 0$  the system of second order are:

$$S_{1,2} = -\omega_0 \xi \pm j\omega_0 \sqrt{1-\xi^2} \quad (\text{If } 0 \leq \xi < 1) \tag{9}$$

The characteristic polynomial wanted takes the following form:

$$D(s) = (s^2 + 2\omega_0\xi s + \omega_0^2)(S-S_r) \tag{10}$$

Equation (10) accepts three poles, at least one is real ( $S_r$ ), the other two poles ( $S_{1,2}$ ) are either real (if the discriminant  $\Delta D(s) > 0$ ) or complex conjugate (if  $r$ ). Therefore, to obtain a second order system, we must put  $S_r$  as far as possible in the left half complex plane and place the two complex poles ( $s_{1,2}$ ) the closest possible to the imaginary axis (figure 2). In this case  $s_r$  will have a negligible in response of the controlled PV MPPT parameter ( $v_{pv}$ ).

Therefore, we can write the second condition:

$$|\text{Re}(s_r)| \gg |\text{Re}(s_{1,2})| \tag{11}$$

The denominator  $D(s)$  is a third order polynomial which is in the general form:

$$D(s) = d_3 s^3 + d_2 s^2 + d_1 s + d_0 \tag{12}$$

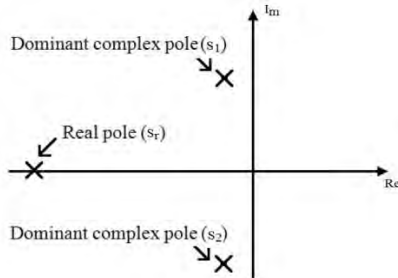


Fig. 2: Location of dominant poles of a second order system

Applying (11) on (10) and (12), we obtain requirements imposed on the coefficients ( $d_0$ ,  $d_1$ ,  $d_2$ , and  $d_3$ ) of (12) for getting a dominant second order system. We obtained the following system of equations:

Based on (13), the values of  $L$ ,  $C_{pv}$  and  $C_0$  will be chose (we respect the CCM as in [5]). The dynamic resistance  $r_{pv}$  defines the operating point on the characteristic V-I and it depends on the temperature and irradiation levels.

$$\left\{ \begin{array}{l} S_r = -d_2 \\ \omega_0 = \sqrt{\frac{d_0}{d_2}} \\ \xi = \frac{d_1 d_2 - d_0}{\sqrt{4d_0 d_2^3}} \end{array} \right. \quad (13)$$

As it is shown in [4], this resistance takes big values if the irradiation takes small values and vice versa. The second parameter (d) defines the transformation ratio between the input and the output of the used converter; it gives the voltage level of the connected load

The first step for having a second order system is to have discriminant  $\Delta D(s) < 0$  whatever the variations in irradiation and temperature levels (the variation interval of  $r_{pv}$ ) and whatever the load variation (the variation interval of d). This condition decides the first interval for dimensioning the elements (L,  $C_{pv}$  and  $C_0$ ).

•Using the **boost** topology

$$F_{V_{pv,d}}(s) = \frac{-\frac{V_{PVE}}{LC_{pv}(1-d)}s - \frac{2V_{PVE}(1-d)}{LC_{pv}C_0r_{pv}}}{s^3 + \left[ \frac{1}{r_{pv}} \left( \frac{(1-d)^2}{C_0} + \frac{1}{C_{pv}} \right) \right] s^2 + \left[ \frac{(1-d)^2}{C_0} \left( \frac{1}{C_{pv}r_{pv}^2} + \frac{1}{L} \right) + \frac{1}{LC_{pv}} \right] s + \frac{2(1-d)^2}{LC_{pv}C_0r_{pv}}} \quad (14)$$

•Using the **buck** topology

$$F_{V_{pv,d}}(s) = \frac{-\frac{V_{PVE}}{C_{pv}dr_{pv}}s^2 - \left( \frac{V_{PVE}}{C_{pv}C_0d^3r_{pv}^2} + \frac{dV_{PVE}}{LC_{pv}} \right) s - \frac{2V_{PVE}}{LC_{pv}C_0dr_{pv}}}{s^3 + \left[ \frac{1}{r_{pv}} \left( \frac{(1-d)^2}{C_0} + \frac{1}{C_{pv}} \right) \right] s^2 + \left[ \left( \frac{1}{C_{pv}C_0d^2r_{pv}^2} + \frac{1}{LC_0} + \frac{d^2}{LC_{pv}} \right) \right] s + \frac{2}{LC_{pv}C_0r_{pv}}} \quad (15)$$

•Using the **buck-boost** topology

$$F_{V_{pv,d}}(s) = \frac{-\frac{V_{PVE}}{C_{pv}dr_{pv}}s^2 - \left[ \frac{V_{PVE}(1-d^2)}{C_{pv}C_0d^3r_{pv}^2} + \frac{d(1-2d)V_{PVE}}{LC_{pv}(1-d)} \right] s + \frac{2V_{PVE}(1-d)^2}{LC_{pv}C_0dr_{pv}}}{s^3 + \left[ \frac{1}{r_{pv}} \left( \frac{(1-d)^2}{C_0d^2} + \frac{1}{C_{pv}} \right) \right] s^2 + \left[ \frac{(1-d)^2}{C_{pv}C_0d^2r_{pv}^2} + \frac{1}{L} + \frac{d^2}{LC_{pv}} \right] s + \frac{2(1-d)^2}{LC_{pv}C_0r_{pv}}} \quad (16)$$

Figure 3 shows the variations of the discriminant ( $\Delta D(s)$ ) for each of the three systems. The intervals of  $r_{pv}$  and d are chosen based on common intervals for which the three systems verify the logical variation interval of  $\xi$  ( $0 \leq \xi \leq 1$ ).

Obviously, for the three cases of PV MPPT system,  $\Delta D(s)$  is negative whatever the values of  $r_{pv}$  and d used in the design of the elements of storage. So the first condition is verified.

The second condition (14) which is to having a very real pole away from the imaginary axis. This condition determines the sub-range of L,  $C_{pv}$  and  $C_0$  of each of the three topologies. Solving (16) gives a relationship between L,  $C_{pv}$  and  $C_0$  for

having a non-dominant real pole. **Table 2** resumes the obtained values of the passive components of each used topology, where:

$f_{sw}$  is the switching frequency (10 kHz);  $\Delta i$  is the inductor current ripple (1%),  $R_{pv}$  and  $D$  are the average values of both of the photovoltaic resistance (20 [ $\Omega$ ]) and duty cycle (0.5) respectively.

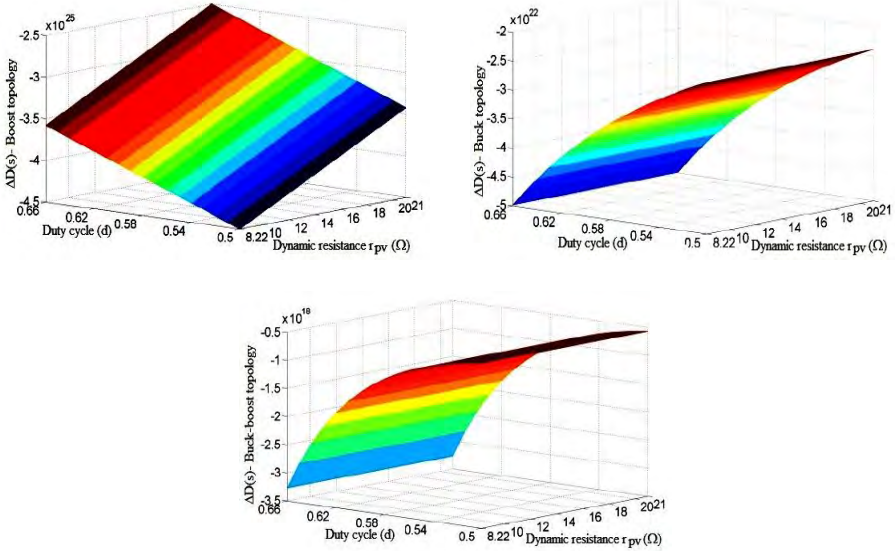


Fig. 3: Variations of the discriminants of the PV MPPT system using boost, buck and buck-boost topologies, respectively

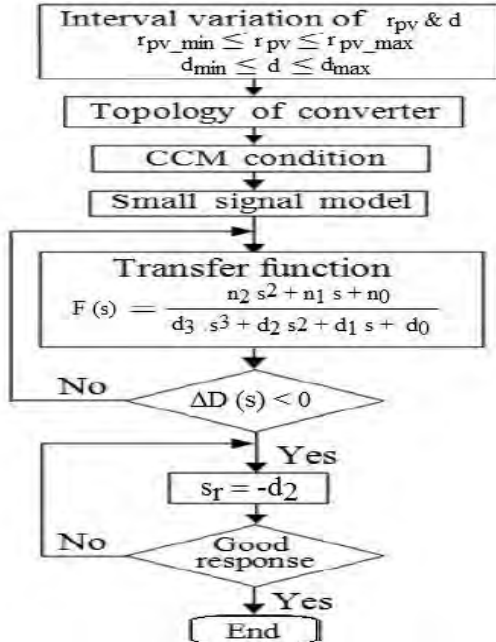


Fig. 4: Algorithm modelling a third order PV MPPT system to a second order

The previous two conditions are grouped in the algorithm of figure 4, which shows the followed steps for obtaining a second order system.

As a result of this mathematical simplification, figure 5 shows the placement of poles and zeros of the transfer function ( $F_{vpv,d}$ ) of each of the three systems. For example if  $r_{pv} = 20\Omega$  and  $d = 0.5$  the placement of the real pole ( $s_r$ ) is as far from the two conjugate poles ( $s_{1,2}$ ) that can neglect its influence on the transient response. **Table 3** shows the obtained values of each pole and zero of the three systems.

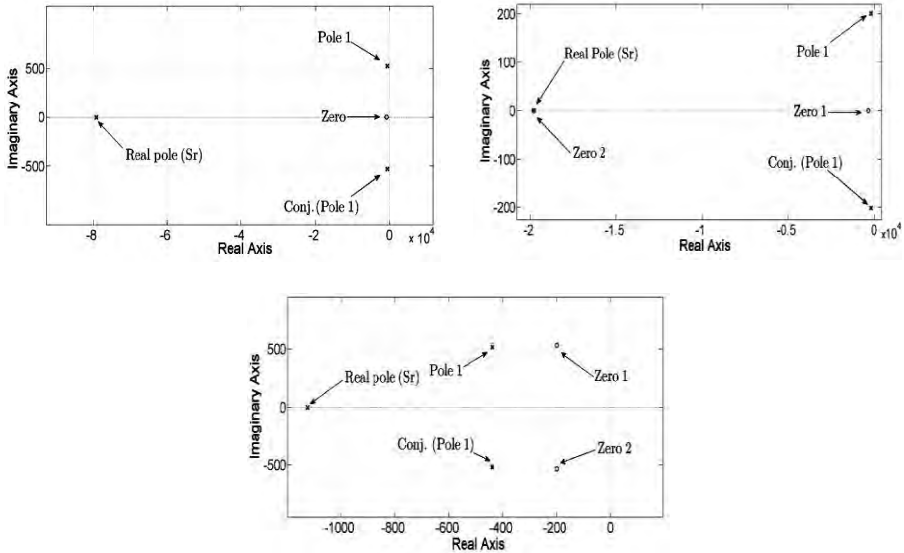


Fig. 5: Location of poles and zeros of the PV MPPT system using boost, buck and buck-boost topologies, respectively

**Table 3:** Obtained values of poles and zeros of three systems

Type converter	Zeros	Poles
<b>Boost</b>	-690.3	$-604.1 \pm j530.7$ and $-7.919 \times 10^4$
<b>Buck</b>	-404.1 and $< -1.98 \times 10^4$	$-201 \pm j201$ and $> -1.98 \times 10^4$
<b>Buck-boost</b>	$-200 \pm j529.2$	$-437.9 \pm j513.5$ and -1124

So in this case, the three systems can be presented by the transfer function of a second order system as shown in figure 6.

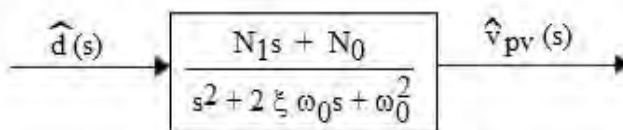


Fig. 6: Transfer function of a second order system

**Table 4** describes the dependence of  $\xi$  and  $\omega_0$  on each of the three system parameters, so we will study the variations of these two latter parameters according to the variations of both  $r_{pv}$  and  $d$ .

**Table 4:** Analytical forms of ( $\omega_0$ ) and ( $\xi$ ) for different converters' topologies

Type de converter	Damping factor ( $\xi$ )	Natural frequency ( $\omega_0$ )
Buck	$\frac{C_{pv}(L + C_{pv}r_{pv}^2)(1-d)^4 + LC_0(1-d)^2 + C_0^2r_{pv}^2}{2r_{pv}(1-d)\sqrt{2L(C_{pv}(1-d)^2 + C_0)^3}}$	$(1-d)\sqrt{\frac{2}{L(C_{pv}(1-d)^2 + C_0)}}$
Boost	$\frac{C_0^2r_{pv}^2d^6 + (C_{pv}^2r_{pv}^2 + C_0L)d^2 + C_{pv}L}{2r_{pv}d(1-d)\sqrt{2L(C_{pv}(1-d)^2 + C_0d^2)^3}}$	$d\sqrt{\frac{2}{L(C_{pv} + C_0d^2)}}$
Buck boost	$\frac{C_0^2r_{pv}^2d^6 + C_{pv}(L + C_{pv}r_{pv}^2d^2)(1-d)^4 + C_0Ld^2(1-d)^2}{2r_{pv}d(1-d)\sqrt{2L(C_{pv}(1-d)^2 + C_0d^2)^3}}$	$d(1-d)\sqrt{\frac{2}{L(C_{pv}(1-d)^2 + C_0d^2)}}$

### 3. CRITERIA OF THE TRANSIENT RESPONSE

In the previous section, the second order system is obtained based on a mathematical simplification of the third order system, and we obtained the formulas of the parameters  $\xi$  and  $\omega_0$ .

In a second order system, the parameters  $\xi$  and  $\omega_0$  characterize the step transient response (figure 7).

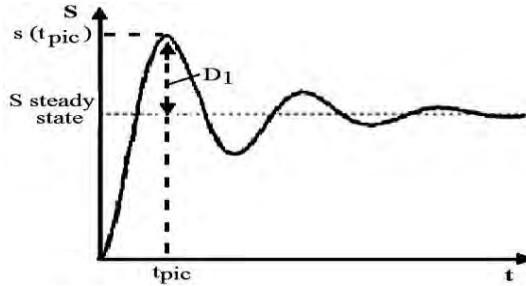


Fig. 7: Transient response to a step

This transient response is characterized by the first overtake ( $D1$ ), which reflecting the degree of damping of the system and the first peak time ( $t_{pic}$ ), which reflecting the rapid transient. Generally, it is desired to obtain a fast transient and well damped, therefore a more optimized real time MPPT algorithm.

The first overtake ( $D1$ ) and time to peak ( $t_{pic}$ ) of the transient are directly related to  $\xi$  and  $\omega_0$  by the following relationships [9]:

$$t_{pic} = \pi / (\omega_0 \sqrt{1 - \xi^2}) \quad (17)$$

$$D1 = 100 \exp\left(-\frac{\pi \xi}{\sqrt{1 - \xi^2}}\right) \quad (18)$$

### 4. RESULTS OF THE ANALYTICAL STUDY

In the following as it is indicated in figure 6, we will show in subsections A and B the variation of  $\xi$  and  $\omega_0$  respectively for the three systems, then in subsection C the influence of  $\xi$  and  $\omega_0$  variations on the output PV voltage  $v_{pv}$  through  $D1$  and  $t_{pic}$  variations.

#### 4.1 Discussion about the damping factor ( $\xi$ )

Based on control theory of linear systems, a good sizing of  $\xi$  ( $\approx 0.703$ ) minimizes the oscillations of the system in the transitional phase by decreasing  $D1$  which implies a will damped system so the corresponding losses will be reduced when the MPPT action.

According to **Table 4**, the obtained analytical form of the damping factor ( $\xi$ ) for the three systems depends on both of  $d$  and  $r_{pv}$ . Figure 8 shows these variations for the three PV MPPT systems when using the boost, buck and buck-boost topologies.

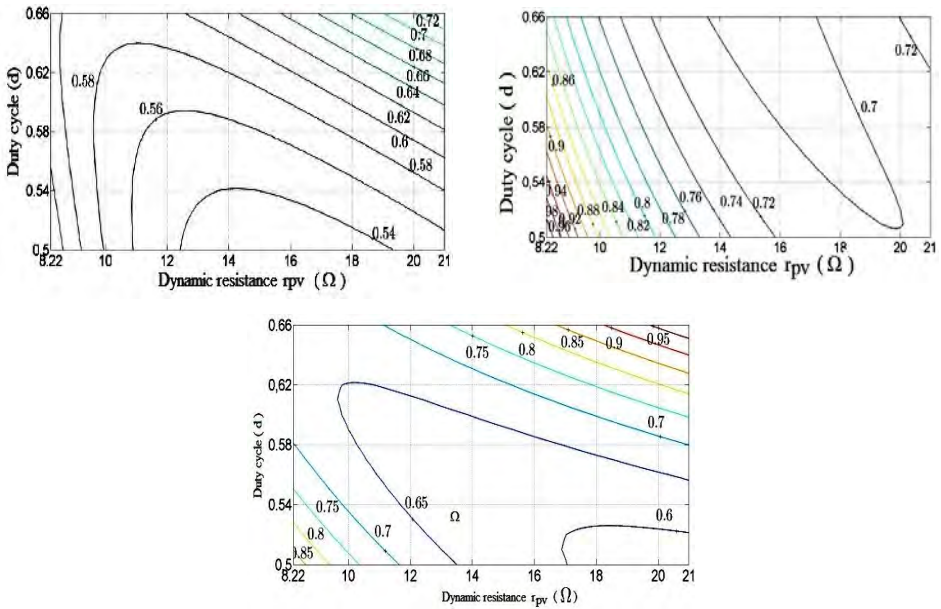


Fig. 8: Damping factor ( $\xi$ ) variations of the PV MPPT system using boost, buck and buck-boost topologies, respectively vs.  $d$  &  $r_{pv}$

#### 4.2 Discussion about the natural frequency ( $\omega_0$ )

A good sizing of  $\omega_0$  reduces the system time response that implies fast MPPT reactions. Based on **Table 4**, it is found that the analytical form of  $\omega_0$  depends only on  $d$ . Figure 9 shows its variations for the three cases of PV MPPT system.

#### 4.3 Criteria of the transient response

The criteria of the transient response ( $t_{pic}, D1$ ) are indirectly related to the variations of both  $r_{pv}$  and  $d$  through the variation of  $\xi$  and  $\omega_0$ .

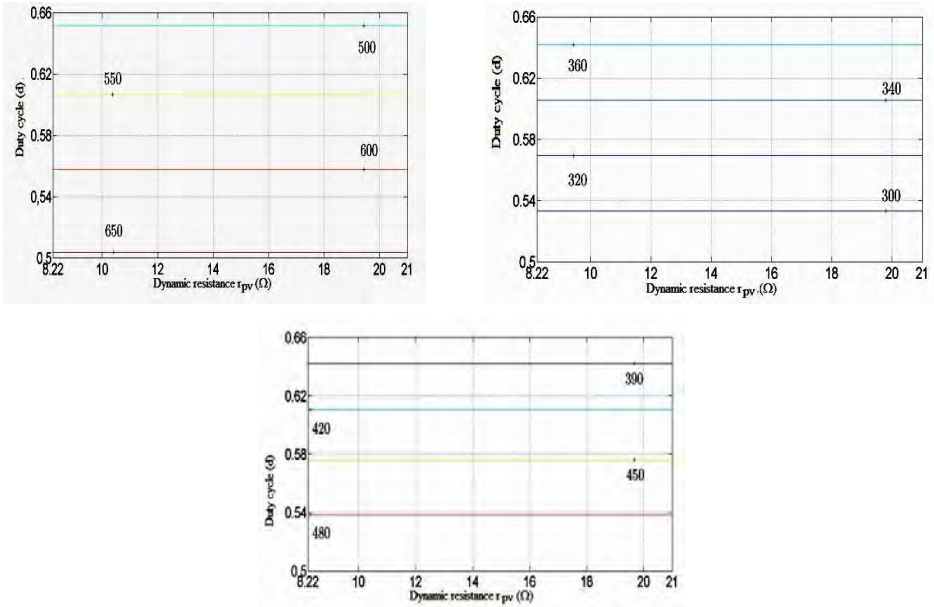


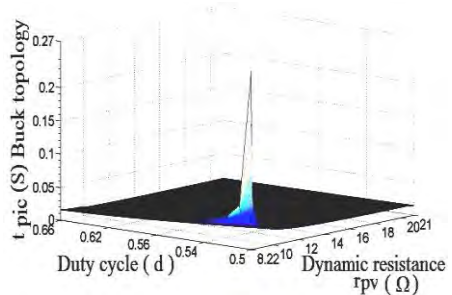
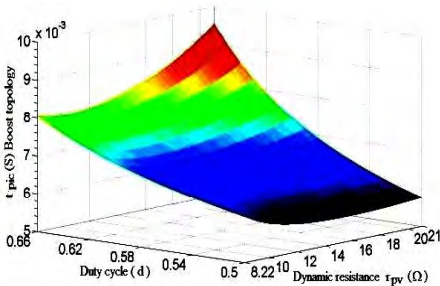
Fig. 9: Variations of the natural frequency  $\omega_0$  (rad/s) of the PV MPPT system using boost, buck and buck-boost topologies, respectively vs.  $d$  &  $r_{pv}$

**4.3.1 The first peak time ( $t_{pic}$ )**

The formula (17) shows that  $t_{pic}$  depends on both  $\xi$  and  $\omega_0$ , so its variations are indirectly influenced by the variations of  $r_{pv}$  and  $d$ .

After figure 10, the obtained values for the three systems are translated that  $\omega_0$  has a more influence than  $\xi$  on  $t_{pic}$  variations, which implies that  $d$  is the more important parameter that influences the duration of  $t_{pic}$ .

Adding to that, from the same figure, and based on the proposed analytical approach, it is found that  $t_{pic}$  of the PV MPPT system when using the boost topology is the shortest {approximated variations from 6 to 10 (ms)} following by that of buck-boost then of buck topologies.



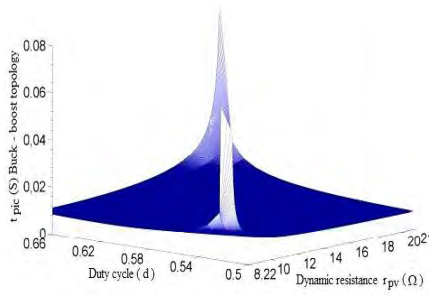


Fig. 10: Variations of the first peak time  $t_{pic}$  (s) of the output PV voltage  $v_{pv}$  using boost, buck and buck-boost topologies, respectively vs.  $d$  &  $r_{pv}$

### 4.3.2 The first overtake (D1)

According to (18), the first overtake (D1) depends only on  $\xi$  which means that the two parameters  $r_{pv}$  and  $d$  have an influence on its variations.

After figure 11, it is found that D1 of the PV MPPT system when using the buck topology is the best one {approximate variations from 0.5 to 4 % to the  $v_{pv}$  steady state value} following by that of buck-boost and then of that of boost topologies.

## 5. CONCLUSION

In this paper, we have presented the dynamic behavior overview of three conventional dc/dc converter topologies used in PV MPPT system. The transfer function ( $F_{V_{pv},d}$ ) is obtained and its mathematical simplification to the second order is used for the case of boost, buck and buck-boost topologies.

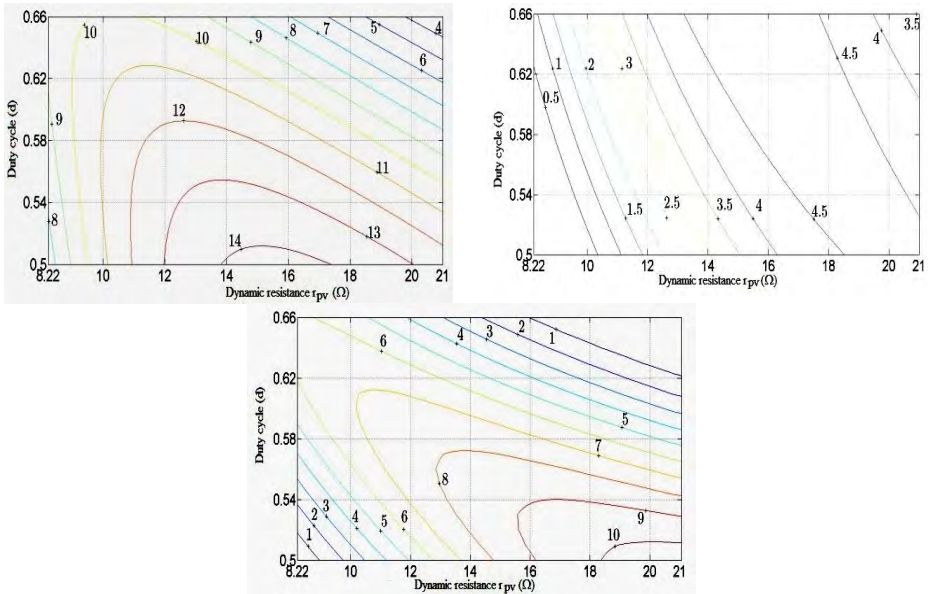


Fig. 11: Variations of the first overtake  $D1$  (% to the  $v_{pv}$  steady state value) using boost, buck and buck-boost topologies, respectively vs.  $d$  &  $r_{pv}$

The results of analytical studies based on  $\xi$  and  $\omega_0$  variations, allowed us having an overview about the transient response behavior of the output PV voltage ( $v_{pv}$ ) according to a specified variation interval of both  $r_{pv}$  and  $d$ , and that, by studying the first overtake ( $D1$ ) and time to the first peak ( $t_{pic}$ ).

For the aim to implement a more efficient real-time MPPT algorithm, as the operating point of the PV MPPT system changes with the operating conditions and based on the proposed dynamic behavior study, it is found that the buck topology is the more adequate topology to use in such optimization of perturbative PV MPPT algorithms, since this latter topology shows a middle trade-off between a well damped and fast system when the MPPT action.

## NOMENCLATURE

<b>PV</b> , Photovoltaic	<b>DC</b> , Direct current	<b>AC</b> , Alternative current
<b>MPPT</b> , Maximum power point tracking- $\xi$ , Damping factor	<b>MPP</b> , Maximum power point	<b>PWM</b> , Pulse width modulation
$C_{pv}$ , Input capacitor	$r_{pv}$ , Dynamic resistance	<b>CCM</b> , Continuous conduction mode
$L$ , Inductance	$C_0$ , Output capacitor	<b>S, D</b> , Switching cells
$ \text{Re}(s_1) $ , Absolute value of the real pole. $d$ , Duty cycle	$R_0$ , Output resistance	$\omega_0$ , Natural frequency
$F_{V_{pv,d}}$ , Small-signal control to the PV module voltage transfer function	$ \text{Re}(s_{1,2}) $ , Absolute value of the two conjugate poles	$\Delta d$ , Duty cycle Step change
$T_{sw}$ , Switching period	$D(s)$ , Denominator of the transfer function.	$\Delta D(s)$ , Denominator discriminant
$\Delta i$ , Inductor current ripple	$s_r$ , Real pole,	$d_0, d_1, d_2, d_3$ , Denominator coefficients.
$D1$ , First overtake	$T_s$ , Sampling frequency	$R_0$ , Output resistance
	$s_{1,2}$ , Dominant complex conjugate poles	$T_{pic}$ , Time to peak
		$\hat{v}_0$ , Small ac variations of the output voltage

## REFERENCES

- [1] R. Bründlinger, N. Henze, H. Häberlin, B. Burger, A. Bergmann and F. Baumgartner, 'preEN 50530 – The New European Standar For Performance Characterisation of PV Inverters', 24<sup>th</sup> European Photovoltaic Solar Energy Conference, Hamburg, Germany, September 2009.
- [2] N. Femia, G. Petrone, G. Spagnuolo, and M. Vitelli, 'Optimization of Perturb and Observe Maximum Power Point Tracking Method', IEEE Transactions of Power Electronics, Vol. 20, N°4, pp. 963 - 973, 2005.
- [3] P. Manganiello, M. Ricco, G. Petrone, E. Monmasson, and G. Spagnuolo, 'Optimization of Perturbative PV MPPT Methods through Online System Identification', IEEE Transactions on Industrial Electronics, Vol. 61, N°12, pp. 6812 - 6821, 2014.
- [4] W. Xiao, W. G. Dunford, P. R. Palmer, and A. Capel, 'Regulation of Photovoltaic Voltage', IEEE Transactions Industrial Electronics, Vol. 54, N°3, pp. 1365 - 1374, 2007.
- [5] W. Xiao, N. Ozog, and W.G. Dunford, 'Topology Study of Photovoltaic Interface for Maximum Power Point Tracking', IEEE Transactions Industrial Electronics, Vol. 54, N°3, pp. 1696 - 1704, 2007.
- [6] H. Snani, M. Amarouayache, A. Bouzid, A. Lashab, and H. Bounechba, 'A Study of Dynamic Behaviour Performance of DC/DC Boost Converter used in the Photovoltaic System', in

Proceedings 15<sup>th</sup> IEEE International Conference on Environment and Electrical Engineering, pp. 1966 – 1971, 2015.

- [7] J. Fernando Silva, and S. Ferreira Pinto, ‘Advanced Control of Switching Power Converters’, Power Electronics Handbook (3<sup>rd</sup> Ed.), pp. 1037 - 1113, 2011.
- [8] H.Y. Kanaan, ‘*A Contribution to the Modelling and Control of Unidirectional Fixed Switching-Frequency Unity-Power-factor Boost-Type Three-Phase Rectifiers*’, Ph.D. Thesis, Montréal, Canada, Mars 2002.
- [9] R.D. Middlebrook, and S. Cuk, ‘*A General Unified Approach to Modelling Switching-Converter Power Stages*’, International Journal of Electronics, Vol. 42, N°6, pp. 521 - 550, 1977.